Applied Catalysis B: Environmental 178 (2015) 186–191

Contents lists available at ScienceDirect

Applied Catalysis B: Environmental

journal homepage: www.elsevier.com/locate/apcatb

Ink-jet printed planar electrochemical cells

Petr Dzik[a,b,*], Michal Veselý[a,b], Marcela Králová[b], Michael Neumann-Spallart[c]

[a] Faculty of Chemistry, Brno University of Technology, Purkynova 118, 612 00 Brno, Czech Republic
[b] Central European Institute of Technology, Brno University of Technology, Technicka 3058/10, 616 00 Brno, Czech Republic
[c] Groupe d'Étude de la Matière Condensée (GEMaC), CNRS/Université de Versailles, 45, avenue des États-Unis, 78035 Versailles CEDEX, France

ARTICLE INFO

Article history:
Received 10 July 2014
Received in revised form 28 August 2014
Accepted 13 September 2014
Available online 27 September 2014

ABSTRACT

Planar, interdigitated photoelectrochemical cells were made by ink jet printing. The electrode fingers had widths from 200 to 2000 μm and were revealed by printing a positive protective polymer mask on FTO ($F:SnO_2$) covered glass slides and subsequent etching. One finger family was covered by TiO_2, made by using an ink containing the precursor inside inverted micelles and annealing in air. Due to the interdigitated layout, photoelectrochemical response was not suffering from *iR* drop down to low electrolyte ionic strengths. The photoelectro-catalytic degradation of an aqueous solution of terephthalic acid by UVA illumination and electric bias of 1 V was demonstrated by monitoring the fluorescence of the OH-substituted molecule.

1. Introduction

Photocatalytic systems based on slurried powder of TiO_2 offer excellent performance due to their very high catalyst surface area [1]. Upon immobilization, the free surface of catalyst inevitably decreases, resulting in a loss of catalytic performance due to limited mass transport [2]. Nevertheless, immobilized TiO_2 is the preferred form of photocatalyst for practical application, since the need of separating a suspended powder from the fluid to be purified can prohibitively complicate any process at the industrial scale.

The photocatalytic activity of any immobilized semiconductor photocatalyst can be boosted by the application of external electrical bias [3]. The strategy is based on enhancing the electron–hole separation and consequently increasing the quantum yield of the pollutant degradation by the application of electrical bias, which is possible when the photocatalyst is deposited on an electrically conducting substrate [4–6]. However, in the resulting electrochemical cell, *iR* drop is one of the factors limiting high current throughput at moderate bias. If the treatment of low ionic strength media (drinking water) is envisaged, means for minimizing the *iR* drop must be secured.

One way is to use a parallel plate reactor with two opposite electrodes and a small space between them where the electrolyte is passed through [7]. However, the pressure build-up is considerable in a module consisting of many such cells. This drawback can be avoided by using a planar electrochemical cell with two interdigitated electrodes (IDE). The working electrode consists of an electrical conductor covered by a semiconducting metal oxide (e.g. titanium dioxide). The counter electrode material is not critical as long as sufficient electrical conductivity and corrosion resistance is provided and interdigital geometry is respected. Such a design ensures two key functions: (1) it suppresses the main obstacle to efficient use of absorbed photons, i.e. the recombination of photogenerated charge carriers, by applying external electrical bias to the semiconducting photocatalyst and (2) it avoids the reduction of the generated photocurrent due to *iR* drop, even in electrolytes of low ionic strength. These features make the device an interesting candidate for electrophotocatalytic purification of drinking water. Decomposition of model pollutants has been observed on centimeter-scale prototype devices fabricated by standard lithographic techniques using optical copying through contact masks for resist patterning [8].

Material printing seems to be a promising microfabrication method well applicable for the production of planar layered devices, including interdigitated cells. The technique is based on sequential laying of patterned functional layers by means of modified conventional printing techniques [9]. While generally all traditional printing techniques can be adopted for printing functional layers and patterns, inkjet printing [10] occupies quite a prominent position. Despite its quite narrow viscosity and particle size limits, it seems to be the most suitable technique for lab scale prototype development as no hardware printing form is necessary, i.e., patterns designed on a printer driving computer can be printed directly without the need for physical printing form manufacturing. Moreover, up-scaling is very smooth and easy, because industrial inkjet printers with several meters working width are readily

* Corresponding author. Tel.: +420 541149411.
E-mail address: petr@dzik.cz (P. Dzik).

http://dx.doi.org/10.1016/j.apcatb.2014.09.030
0926-3373/

available [11–13], so transfer from prototype level to a small series level is reduced to switching to a bigger printer.

In this paper, we adopt the principle of planar electrochemical cells to the versatile method of ink-jet printing allowing for rapid processing and essentially unlimited upscaling, and report on the design and technology of planar interdigitated photoelectrochemical cells. We employed a mixed subtractive and additive approach and deposited all the functional and auxiliary layers solely by inkjet printing. The adoption of inkjet printing provided a great freedom in the design of the cells and thus samples of various geometries were easily fabricated. The fabrication procedure is described in this paper in detail, together with the physical, electrochemical and photocatalytic properties of selected cell types.

2. Experimental

2.1. Sample fabrication

Commercial FTO ($F:SnO_2$) coated glass (Sigma–Aldrich) was used as the substrate on which cells were fabricated by a combination of material removal and addition. FTO glass sheets were cut down to 26 × 76 mm slides and cleaned by sonication in Neodisher LM cleaning agent, rinsed in ethanol and fired at 450 °C to burn out any remaining contaminants and activate the surface. In order to adjust the surface energy and wetting behaviour of the printed ink, cooled slides were rinsed in 1 vol% ethanolic solution of an aliphatic hydrocarbon based hydrophobization agent (Toko Waterstop, Tokowax, Switzerland), dried with a stream of nitrogen, rinsed in 1 vol% aqueous solution of sodium dodecylbenzene sulfonate (Enaspol Inc., Czech republic) and dried again.

Printing of all functional and auxiliary layers was performed with an experimental inkjet printer Fujifilm Dimatix 2831. The printer features a disposable 16-nozzle piezoelectric jetting printhead coupled with a 2 mL polyethylene ink tank. It is capable of printing on A4 size substrates with a resolution of up to 5080 dpi, i.e. 5 μm. Both substrate and printhead can be heated in order to speed up solvent evaporation and reduce ink viscosity, respectively. A stroboscopic camera provides still images or slow-down video for the observation of drop formation process, while another fiducial camera is used for precise substrate positioning and aligning of subsequently print layers. The printer has been successfully employed for the deposition of a wide variety of functional and auxiliary layers [14–21] and during the past years has *de facto* become the industrial standard tool for ink development and testing.

Generally, the following procedure was repeated for each printing step: the prepared printing formulations (see below) were sonicated for 5 min and then loaded into syringes. 0.45 μm membrane filters (Pall Corporation, USA) and blunt needles were attached to the syringe luer ports. The printing formulations were filtered and filled into the Dimatix ink tanks. Dimatix 10 pL printing heads were attached to the tanks and sequentially mounted into the Dimatix printer. The drop formation characteristics of all formulations were checked by means of a built-in stroboscopic camera and interaction of the printed material with the substrate was observed by an optical microscope. The interdigitated electrode base pattern as well as the patterns for other layers were drawn as vector graphics and exported to 1-bit BMP files to be used for driving the printer. The electrode fingers had widths ranging from 200 to 2000 μm.

First, the FTO base pattern serving as the current collecting interdigitated electrode was revealed by printing a positive protective polymer mask on the FTO glass slides and subsequent etching. The polymer mask was printed by a commercial UV-curable ink (Svang Cyan, Grapo Ltd., Czech Republic), cured off-line under a mercury vapor medium pressure lamp (25 J/cm^2), and baked on a hot plate at 250 °C for 10 min. Next, the FTO slide was etched in a mixture of zinc powder and 15% aqueous HCl in order to remove the naked FTO while preserving those areas covered by the protective printed mask. After the etching operation was finished, the mask was lifted by burning in a furnace at 450 °C for 30 min.

The second layer, i.e. the titania working electrode, was printed using our previously developed reverse micelles sol–gel composition [18]. However, this time sol concentration was adjusted (0.6 mol of Ti/dm^3) in order to gain easier control over the resulting thickness and cracking. With this adjustment, the final thickness of the titania layer after calcination was 50 nm per single layer. We found that it was possible to print 2 layers of sol in wet-to-wet manner followed by single calcination (heating rate 3 °C per min, 30 min at 450 °C) yielding 100 nm titania layers without any cracking in one deposition cycle. Attempts to print more sol layers followed by single calcination resulted in cracked and/or peeling layers. Therefore, thicker layers need to be prepared by repeating the complete cycle of printing double sol layers and calcination.

The device was finalized by printing a masking frame around its edges defining the active area. The same UV curable ink and curing procedure was employed for this task. Proper aligning of the titania active layer and the insulator mask was achieved by means of the Dimatix fiducial camera, which enables sample observation and print origin alignment with 5 μm accuracy. Fig. 1 summarizes the cell production procedure.

In this manner, devices with electrode finger widths ranging from 200 to 2000 μm were conveniently fabricated. Apart from regularly spaced devices, several other lay-outs were also fabricated and their properties investigated, including reduced gap devices or devices with different finger widths of working and counter electrodes. Moreover, the thickness of the titania working electrode layer was varied in the 100–500 nm range.

2.2. Investigation of IDE device properties

Printed layer quality was monitored by a Nikon Eclipse E200 optical microscope equipped with a polarized light unit and a Nikon D5000 digital camera and a Nikon Camera Control Pro 2 software. SEM imaging and elemental analysis was performed on a ZEISS EVO LS 10 scanning electronic microscope. The same machine was used for layer thickness estimation by observing sample cross sections. Phase composition of calcined titania layers was confirmed by a Panalytical Empyrean XRD system and its diffuse reflectance UV-Vis spectra were recorded by an Ocean Optics Redtide spectrophotometer with a reflectance fiber probe. Layer thickness was investigated by a Dektak XT stylus profilometer.

Photoelectrochemical characterization was performed using a two-electrode setup with the titania overprinted FTO finger family as the working electrode and the opposite naked FTO finger family as the counter electrode. This setup was fitted into a custom-build 15 × 40 × 70 mm quartz cuvette. The cuvette was filled with 0.1 M sodium sulfate solution (15 mS cm^{-1}) and fitted onto an optical bench equipped with a Sylvania Lynx-L 18 W fluorescent UV-A lamp. The lamp emission was monitored by a Gigahertz Optic X97 Irradiance Meter with a UV-3701 probe and the irradiance was set to 5 mW cm^{-2} by adjusting the lamp to cuvette distance. A magnetic stirrer was placed beneath the cuvette and a magnetic flea inside the cuvette provided efficient electrolyte mixing. Electrochemical measurements were performed with a computer controlled electrometer in combination with a National Instruments Labview platform supplying a linear voltage gradient of 5 mV s^{-1} from −0.5 to 2 V. For chopped response curves, the lamp was manually obscured and revealed at 5 s intervals.

Electrophotocatalytic experiments were conducted with the same cell and light source as the electrochemical response curves were measured with. Recently, terephtalic acid was suggested as a model compound for monitoring the oxidative activity of valence

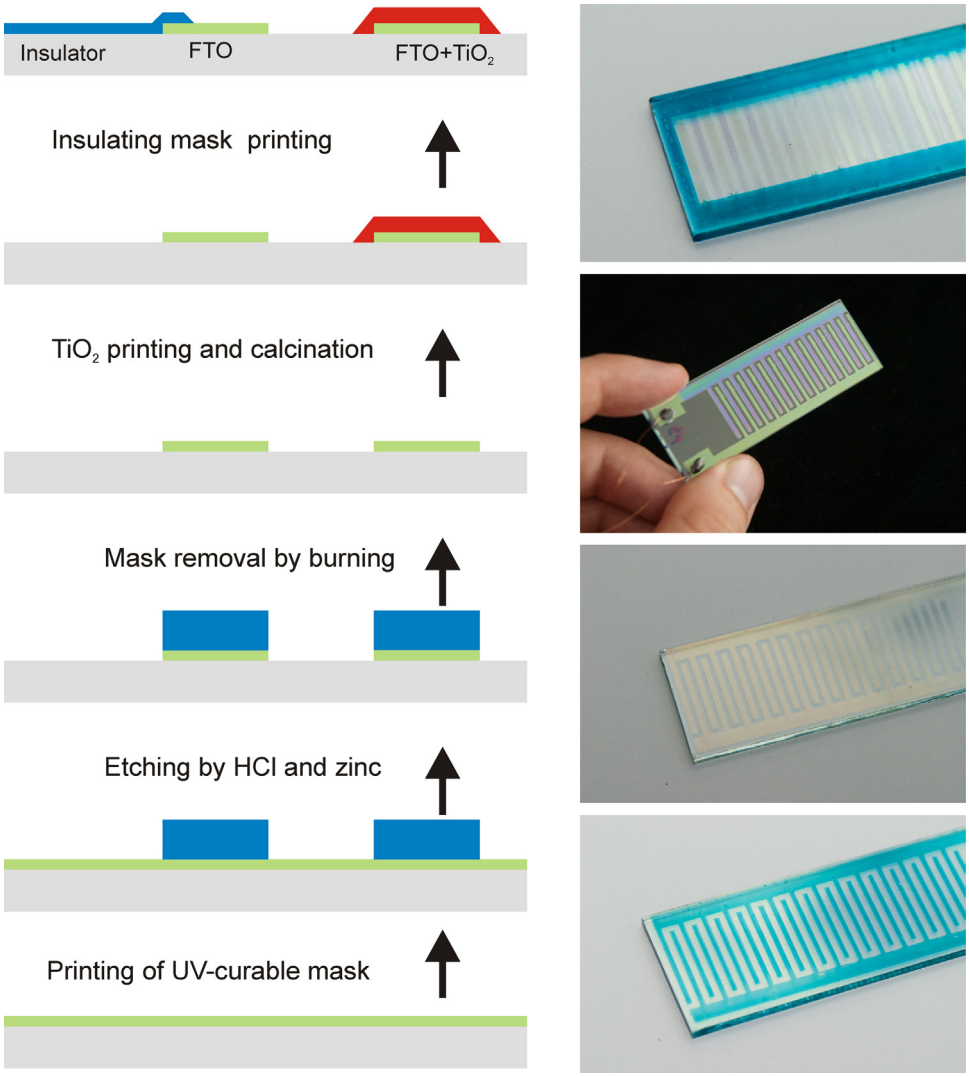

Fig. 1. IDE cell fabrication procedure.

band holes generated in the immobilized photocatalyst [22]. Upon oxidation, presumably resulting from the attack of a hydroxyl radical, terephtalic acid is oxidized into hydroxyterephtalic acid, which gives a strong fluorescence signal at 425 nm. This approach proved to be very convenient for our experimental setup, because a single radiation source could be used for both the activation of the photocatalyst as well as the excitation of the fluorescent probe generated during the course of the reaction. The emitted fluorescence was collected by a quartz collimating lens mounted in the lateral wall of the cell holder and projected into an optical fiber attached to an Ocean Optics Redtide spectrometer. The spectrometer driving software allowed for a convenient automated recording of the fluorescence intensity. Calibration was performed using hydroxyterepthalic acid standard (Sigma–Aldrich).

3. Results and discussion

3.1. Optimization of printing conditions

During inkjet printing on a nonporous, nonabsorbing surface, the surface tension of printed ink and the surface energy of the substrate must closely match in order to ensure optimal wetting behaviour and smooth, but well defined wet layer formation [23]. If the printed liquid is wetting the surface too much, excessive positive dot gain or even pattern bleeding [24] may occur. On the other hand, poor wetting of substrate by the printed ink results into spontaneous shrinking of the printed ink (negative dot gain), or the formation of a bumpy surface resembling the texture of an orange peel [25–27].

While the printer setup and conditions for flawless patterning of the reverse micelles titania ink had been established in our previous work [18], the UV curable ink workflow needed to be optimized in order to produce well resolved patters and good reproducibility. Fig. 2 depicts the key points of this process: the FTO surface after baking is excessively wetted by the printed ink and heavy ink spreading totally ruins the edges of the printed pattern (a). After treatment with the dewetting agent, ink spreading is avoided, but ink is actually dewetting the surface too much and the printed pattern size is reduced (b). Finally, the best results were obtained by treating the FTO glass with the dewetting agent followed by rinse in dodecylbenzene sulfonate, which resulted into just the right degree of wetting producing excellent rendition of even the finest lines down to 100 μm (c).

3.2. Physical properties of devices

For routine checking during sample fabrication, optical microscopy is the preferred tool. However, as all the layers are

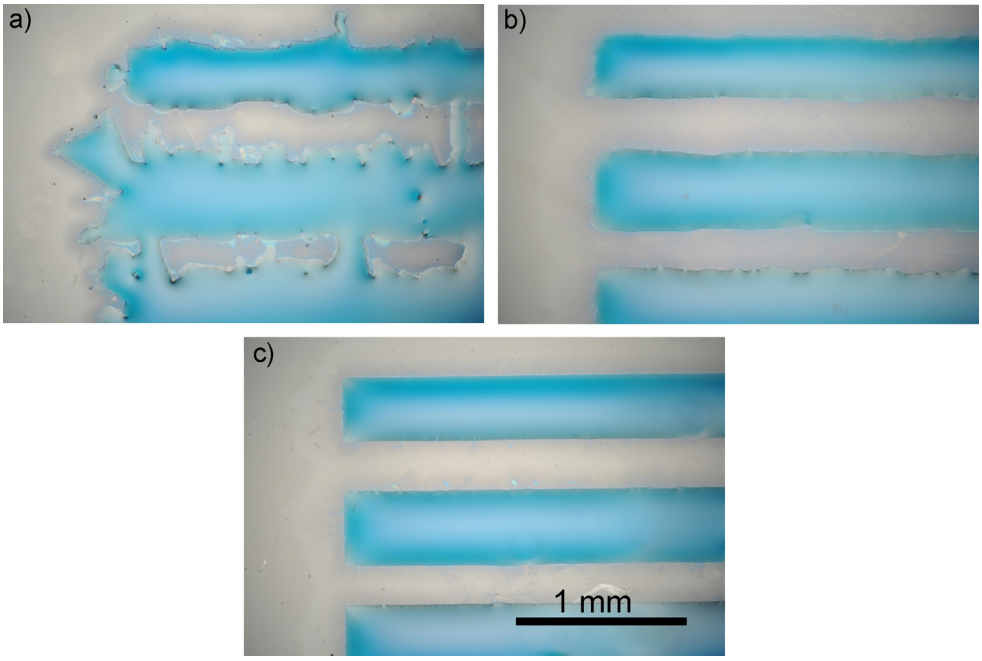

Fig. 2. Influence of substrate treatment on the print quality: (a) FTO surface after baking is excessively wetted by the printed ink with significant positive dotgain and irregular ink bleeding, (b) application of the dewetting agent suppresses ink spreading but ink is actually dewetting the surface too much, resulting into slight negative dotgain, (c) treatment by the dewetting agent plus dodecylbenzene sulfonate produces just the right degree of wetting with excellent definition of pattern edges.

transparent, images tend to be faint and have low contrast. Therefore SEM images are included to depict the device structure. Fig. 3 shows the edge of a finger covered by titania layer. Titania fingers have been designed intentionally 10% wider (1100 and 550 μm) in order to ensure complete coverage of the FTO fingers as well as their edges. This overlap is clearly visible in the middle darkest band of Fig. 3(a). In the same figure we can also observe that the FTO edge is not particularly smooth, which is probably the result of under-etching by the aggressive FTO etching bath. It seems that with the present etching process the minimum width of FTO patterns is limited to approximately 100 μm. The cross-sectional view of the finger confirms the smoothness and evenness of the titania coating resulting from previous optimization.

Profilometric scanning over the centre part of the device reveals repeating units of "titania finger - insulating space - counter electrode finger (FTO) - insulating space". Fig. 4 depicts the record of a stylus profilometric scan across 2 fingers of a 1000–1000–1000–1000 μm device fabricated with 4 cycles of titania deposition. The thickness of the FTO finger (left part of the trace, approximately 250 nm) and of the FTO + titania layer (right part of the trace, approximately 400 nm) can be exactly determined and the overlap of the wider titania strip is also clearly visible. Figs. 5 and 6 illustrate the optical properties and phase composition of the reverse micelles originated titania layers. Strong interference coloring observed visually expresses itself in the typical periodic peaks in the diffuse reflectance spectra. The phase composition was investigated by XRD and the presence of pure anatase phase was confirmed. Further details about the properties of this particular type of titania coating can be found in our previous communication [28].

3.3. Photoelectrochemical properties

The (conductivity) cell constants, κ, of the interdigitated finger device were close to the ones calculated using ref. [29]. A structure of 200 μm wide fingers and spaces was already fine enough to obtain a κ value below 0.01 cm^{-1}. The cells reported in this study,

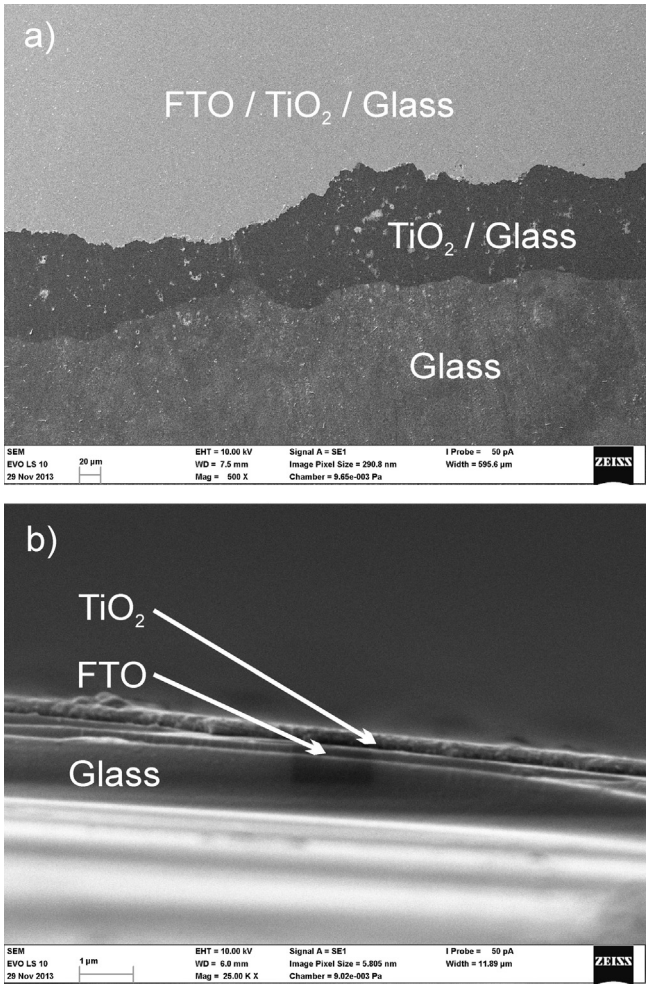

Fig. 3. SEM images of the IDE cells: (a) top view of the boundary of FTO finger overprinted by titania, (b) cross-section of a finger.

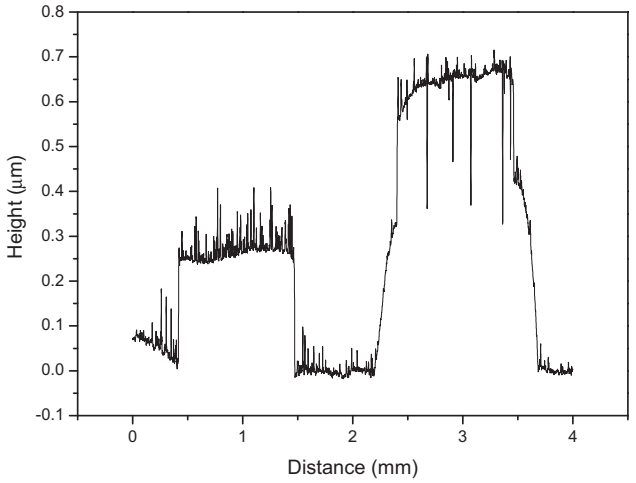

Fig. 4. Profilometric scan of a pair of fingers on a 1000–1000–1000–1000 μm device with 4 cycles of titania deposition yielding an approximately 400 nm thick titania coating.

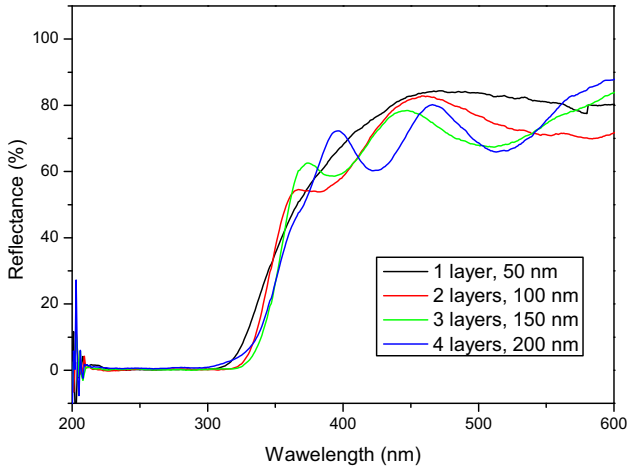

Fig. 5. Diffuse reflectance spectra of printed titania layers.

i.e. cells with 500 and 1000 μm wide fingers, featured cell constants of 0.0136 and 0.0271 cm^{-1}, respectively. A typical photoelectrochemical response of one of the finger devices in two different electrolytes of different conductivity is shown in Figs. 7 and 8. Finer fingers in the case of the 500 μm device result in lower cell

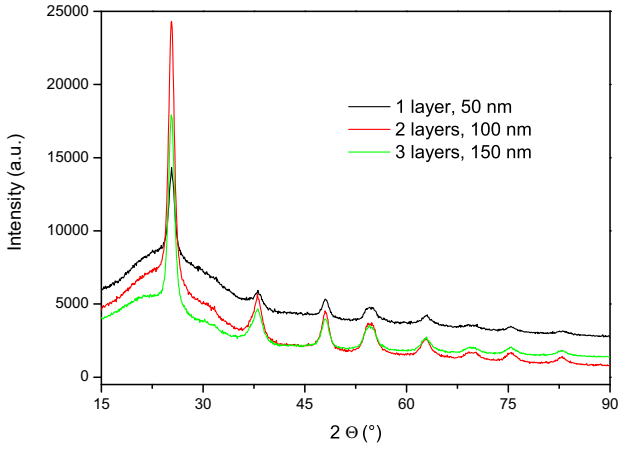

Fig. 6. XRD patterns of TiO_2 films, Cu-K_α irradiation.

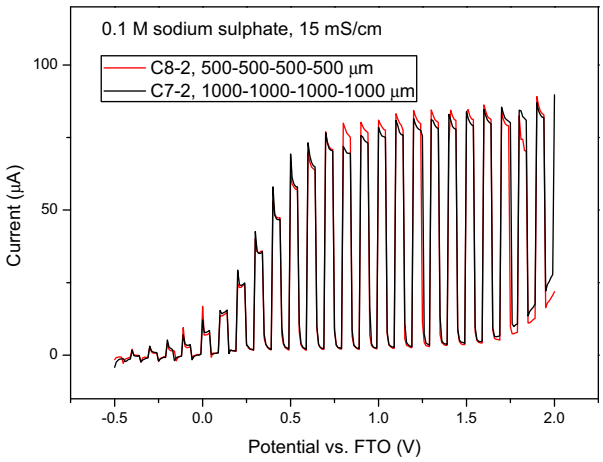

Fig. 7. Chopped photocurrent response curve in sodium sulfate electrolyte.

constants, which are beneficial for suppression of *iR* drop in electrolytes of low conductivities.

3.4. Electrophotocatalysis

Finally, an example of photodegradation of a solution of terephthalic acid under UVA irradiation and assisted by electrical bias, using a 1000–1000–1000–1000 device with 200 nm thick TiO_2 fingers is shown at Fig. 9. During the course of the experiment, the fluorescence due to an intermediary product (OH-substituted) increased and would eventually decrease down to zero as the fluorescent intermediate is further oxidised. The fluorescence at 425 nm plotted as a function of time reflects the initial reaction rate. While the blank checks show essentially no reaction, we can observe a doubling of the reaction rate (with respect to the unbiased case) when an external bias of 1 V was applied. From the initial slopes of the traces, the production rates, v, can be calculated taking into account the total volume of the solution. These production rates, considering Farday's law of electrolysis, are related to the electrical charge passed (photocurrent, i_{photo}). The Faradaic efficiency, f, of the process is calculated using $f = vF/i_{photo}$. The value of 0.009 obtained for the experiment shown in Fig. 9 is satisfactory given the fact that a very low concentration of electroactive species (1.10^{-5} M) was used. Polychromatic light centered at 365 nm was used for this experiment. The IPCE (incident photon-to-current

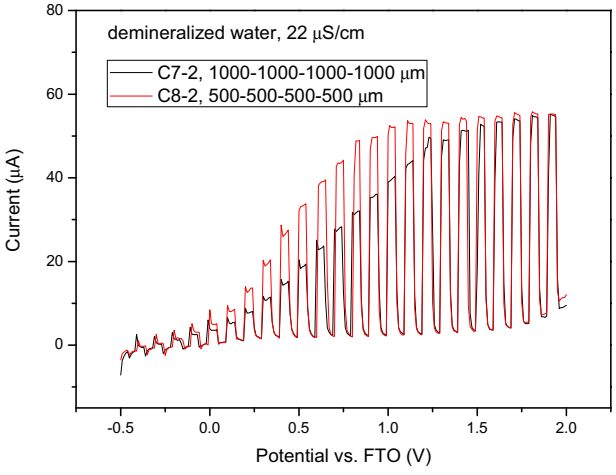

Fig. 8. Chopped photocurrent response curve in demineralized water.

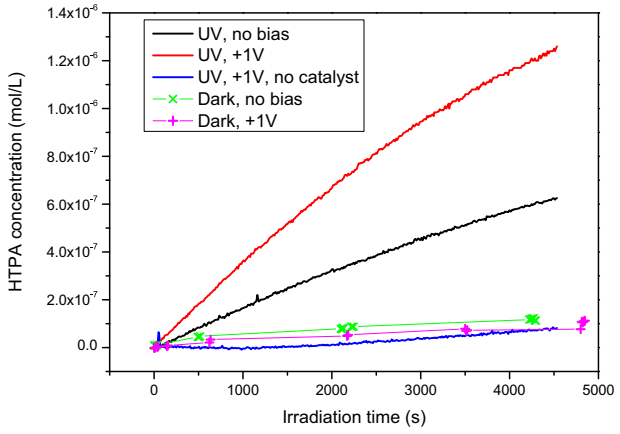

Fig. 9. Concentration profiles of HTPA under various experimental conditions.

efficiency) was 0.13 at 365 nm for 200 nm thick electrodes. Values of *f* were found close to values obtained for the degradation of phthalic acid in a parallel plate reactor [30]. While the datasets of the irradiated samples were measured continuously in 10 s intervals, the dark ones needed to be measured discontinuously only a few times during the reaction duration because a single radiation source was used for both catalyst activation and fluorescent probe excitation.

4. Conclusion

Inkjet material printing was successfully employed for the fabrication of planar interdigitated photoelectrochemical cells. A mixed subtractive and additive approach was adopted and all the functional and auxiliary layers were printed by an experimental inkjet printer Fujifilm Dimatix 2831. Inkjet printing proved to be an elegant method for sol delivery to the substrate. It provides a complete control over the deposition process parameters together with an excellent efficiency of precursor use. Wetting issues associated with the substrate-ink interfacial interactions were controlled by substrate treatment with suitable surfactants.

The process of FTO patterning by etching with the help of a protecting printed mask is very convenient and can be easily adopted for pattering of other materials as well. Although the resolution of printed masks can not compete with the well established resist technologies, it may be well suited for the fabrication of large footprint devices requiring a low degree of integration (solar cells, electroluminescent modules etc.). The absence of a resist development step makes the fabrication process much more environment friendly. Moreover, it does not require any special material or equipment as it can be performed with ordinary flatbed or roll printers and UV-curable inks.

Devices with regular finger arrangement and widths ranging from 200 to 2000 μm were conveniently fabricated and so were several other lay-outs including reduced gap ones or devices with different finger widths of working and counter electrodes. The benefits of finer fingers are clearly demonstrated, resulting in lower cell constants which are beneficial for the suppression of *iR* drop in electrolytes of low conductivities. With the present technology, 200 μm fingers seem to be fine enough for work with electrolytes with ionic strength typical for drinking water.

Comparative photocatalytic and electrophotocatalytic experiments with terephtalic acid as model contaminant compound proved the beneficial role of external electrical bias in suppressing photogenerated electron-hole recombination in the semiconducting photocatalyst. In this way, more efficient charge separation in the electric field of the IDE device has been demonstrated by the acceleration of terephtalic acid oxidation, which was conveniently monitored by the fluorescent signal of its dominant oxidation product, hydroxyterephtalic acid.

Acknowledgements

The authors thank the Technology Agency of the Czech Republic for support through project TA03010548 and the Ministry of Education, Youth and Sports of the Czech Republic for support through project CZ.1.07/2.3.00/30.0005.

References

[1] R. van Grieken, J. Marugan, C. Sordo, C. Pablos, Catal. Today 144 (2009) 48–54.
[2] M. Tasbihi, C.R. Ngah, N. Aziz, A. Mansor, A.Z. Abdullah, L.K. Teong, A.R. Mohamed, Ind. Eng. Chem. Res. 46 (2007) 9006–9014.
[3] M. Neumann-Spallart, Chimia 61 (2007) 806–809.
[4] G. Waldner, A. Bruger, N.S. Gaikwad, M. Neumann-Spallart, Chemosphere 67 (2007) 779–784.
[5] P. Fernandez-Ibanez, S. Malato, O. Enea, Catal. Today 54 (1999) 329–339.
[6] I.M. Butterfield, P.A. Christensen, A. Hamnett, K.E. Shaw, G.M. Walker, S.A. Walker, C.R. Howarth, J. Appl. Electrochem. 27 (1997) 385–395.
[7] P.S. Shinde, P.S. Patil, P.N. Bhosale, A. Bruger, G. Nauer, M. Neumann-Spallart, C.H. Bhosale, Appl. Catal. B-Environ. 89 (2009) 288–294.
[8] M. Neumann-Spallart, Electrochim. Acta 56 (2011) 8752–8757.
[9] F.C. Krebs, Sol. Energ. Mater. Sol. Cells 93 (2009) 394–412.
[10] G.D. Martin, S.D. Hoath, I.M. Hutchings, Iop, Inkjet printing - the physics of manipulating liquid jets and drops Conference on Engineering in Physics - Synergy for Success, London, ENGLAND, 2006.
[11] P. Calvert, Chem. Mater. 13 (2001) 3299–3305.
[12] H. Sirringhaus, T. Shimoda, MRS Bull. 28 (2003) 802–806.
[13] E. Tekin, P.J. Smith, U.S. Schubert, Soft Matter 4 (2012) 703–713.
[14] W. Tang, L.R. Feng, J.Q. Zhao, Q.Y. Cui, S.J. Chen, X.J. Guo, J. Mater. Chem. C 2 (2014) 1995–2000.
[15] M.W. Wang, D.C. Pang, Y.E. Tseng, C.C. Tseng, J. Taiwan Inst. Chem. Eng. 45 (2014) 1049–1055.
[16] G. Tarapata, M. Marzecki, in: R.S. Romaniuk (Ed.), Photonics Applications in Astronomy, Communications, Industry, and High-Energy Physics Experiments 2013, 2013.
[17] J.T. Kwon, S.H. Eom, B.S. Moon, J.K. Shin, K.S. Kim, S.H. Lee, Y.S. Lee, Bull. Korean Chem. Soc. 33 (2012) 464–468.
[18] P. Dzik, M. Morozova, P. Kluson, M. Vesely, J. Adv. Oxid. Technol. 15 (2012) 89–97.
[19] J.D. Swartz, L.F. Deravi, D.W. Wright, Adv. Func.l Mater. 20 (2010) 1488–1492.
[20] E. Sowade, J. Hammerschmidt, T. Blaudeck, R.R. Baumann, D. Polster, T. Baumgartel, H. Graaf, C. von Borczyskowski, R. Wagner, F. Cichos, SIST, Inkjet printing of polymer microspheres, in: NIP 25: Digital Fabrication 2009, Technical Program and Proceedings, 2009, pp. 788–790.
[21] L.F. Deravi, J.D. Swartz, D.W. Wright, Piezoelectric inkjet printing of biomimetic surfaces for enzyme encapsulation, in: D. Schulze Hagenest (Ed.), NIP24/Digital Fabrication 2008: 24th International Conference on Digital Printing Technologies, Technical Program and Proceedings, 2008, pp. 504–507.
[22] U. Cernigoj, M. Kete, U.L. Stangar, Catal. Today 151 (2010) 46–52.
[23] E. Chow, J. Herrmann, C.S. Barton, B. Raguse, L. Wieczorek, Anal. Chim. Acta 632 (2009) 135–142.
[24] S.C.L. Sousa, A.D. Mendes, P.T. Fiadeiro, A.M.M. Ramos, Ind. Eng. Chem. Res. 53 (2014) 4660–4668.
[25] J.A. Roper, R. Urscheler, P. Salminen, E. Moore, R. Tappi, Metered Size Press Forum Ii, Tappi Proceedings, 1998, pp. 37–55.
[26] G. KigleBoeckler, Tappi J. 79 (1996) 194–198.
[27] M. Matsuta, J. Coat. Technol. 59 (1987) 61–64.
[28] M. Morozova, P. Kluson, J. Krysa, P. Dzik, M. Vesely, O. Solcova, Sensor. Actuat. B-Chem. 160 (2011) 371–378.
[29] W. Olthuis, W. Streekstra, P. Bergveld, Sensor. Actuat. B-Chem. 24 (1995) 252–256.
[30] M. Neumann-Spallart, S.S. Shinde, M. Mahadik, C.H. Bhosale, Electrochim. Acta 111 (2013) 830–836.